Classical analog of the Unruh effect

Ulf Leonhardt,[1] Itay Griniasty,[1] Sander Wildeman,[2] Emmanuel Fort,[2] and Mathias Fink[2]
[1]*Weizmann Institute of Science, Rehovot 761001, Israel*
[2]*Institut Langevin, ESPCI, CNRS, PSL Research University, 1 Rue Jussieu, F-75005 Paris, France*

(Received 7 September 2017; revised manuscript received 30 November 2017; published 13 August 2018)

In the Unruh effect an observer with constant acceleration perceives the quantum vacuum as thermal radiation. The Unruh effect has been believed to be a pure quantum phenomenon, but here we show theoretically how the effect arises from the correlation of noise, regardless of whether this noise is quantum or classical. We demonstrate this idea with a simple experiment on water waves where we see the first indications of a Planck spectrum in the correlation energy.

DOI: 10.1103/PhysRevA.98.022118

I. INTRODUCTION

Imagine an observer moving through the quantum vacuum of empty space. In free space, the quantum vacuum is Lorentz invariant, so a uniformly moving observer would not see any effect due to motion, but an accelerated observer would. This is known as the Unruh effect [1] (or Fulling-Davies-Unruh effect in full [1–3]). An observer with constant acceleration a is predicted [1] to perceive empty space as thermal radiation with Unruh temperature,

$$k_{\mathrm{B}}T = \frac{\hbar a}{2\pi c}, \tag{1}$$

where c is the speed of light in vacuum, $\hbar$ Planck's constant divided by 2π, and k_{B} Boltzmann's constant.

The Unruh effect and the closely related Bekenstein-Hawking radiation of black holes [4,5] has been one of the most important results of theoretical physics of the second half of the 20th century, hinting of a hidden connection between three vastly different areas of physics indicated by the constants appearing in Eq. (1): general relativity (acceleration a versus c), quantum mechanics ($\hbar$), and thermodynamics (k_{B}). It has been the benchmark for theories attempting to unify these areas ever since.

Yet there has been no experimental evidence for the Unruh effect. The reason becomes evident if one puts numbers into Unruh's formula: With $\hbar \approx 10^{-34}$Js and $c \approx 3 \times 10^{8}$ m/s one needs an acceleration of about 10^{23} m/s^2 to reach room temperature. Three avenues [6] have been suggested for getting closer to an observation of Unruh radiation: (i) strong-field acceleration such as in laser plasmas, wake fields, or strongly accelerated electrons, (ii) cavity QED, and (iii) particle accelerators; none have been successful so far.

Here we propose and experimentally demonstrate a classical analog of the Unruh effect, where $\hbar$ is replaced by the strength of classical noise and c by the speed of the waves involved in the effect. In our case (Fig. 1) these are water waves with c of about 0.2m/s. In this way, the Unruh temperature of Eq. (1) is boosted such that the Unruh effect becomes observable. Furthermore, we have solved some fundamental challenges all Unruh measurements face: how to perform measurements of the Unruh spectrum in confined, finite space and in finite time.

Analogs [7] of the Unruh effect have been proposed before: the use of impurities in Bose-Einstein condensates as accelerated particle detectors [8] or of graphene [9] folded into a Beltrami trumpet [10] that corresponds to an accelerate space. It was also suggested [11] to employ a quantum simulator made of cold atoms in an optical lattice to generate a synthetic Unruh effect in arbitrary dimensions [12]. So far, none of these ideas, exciting as they are, were experimentally demonstrated. Connections between the Unruh effect and classical physics have also been pointed out before [13–16], but not the simple connection we found.

One advantage of our scheme is its simplicity. Figure 1 illustrates the principal idea; the actual experiment is modified and described in Sec. III. Imagine a container filled with water subjected to white noise. The resulting ripples on the water surface are scanned with a movable laser beam, while a camera is taking a video of the height of the illuminated spot [17,18]. The moving spot plays the role of the moving detector; the water ripples represent the vacuum noise. The spot should move along the space–time trajectory (Fig. 2) of an observer with constant relativistic acceleration where c is replaced by the speed of the water waves. The varying height of the water ripples are recorded along the trajectory for each run, and the experiment is repeated many times to get reliable statistics.

Note that the combination of laser spot and video camera acts like an amplitude detector, whereas Unruh [1] considered a particle detector. However, an amplitude detector can, in principle, replace a particle detector: The particle-number distribution is tomographically obtainable from amplitude measurements [19,20]. Note also that in classical physics the interaction between the detector and the detected physical object can be made arbitrarily small, in contrast to quantum physics [19]. It is therefore sufficient to record the ripples on the surface, but not to interact with them. So instead of scanning the waves with a laser beam one could simply take a video of the entire surface and then postselect the data along the space-time trajectory (Fig. 2). This is what we have done in our experiment.

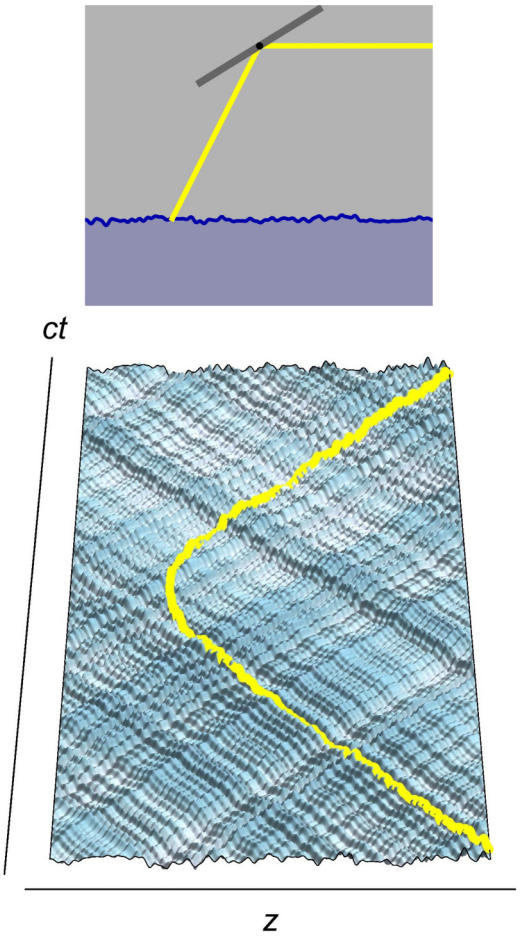

FIG. 1. Principal idea. A container is filled with water subject to noise creating ripples on the water surface. (Top) A movable mirror guides a laser beam over the water surface illuminating a sharp spot recorded by a video camera. (Bottom) Video of the water surface and space-time diagram of the illuminated spot following the trajectory of the accelerated observer (Fig. 2).

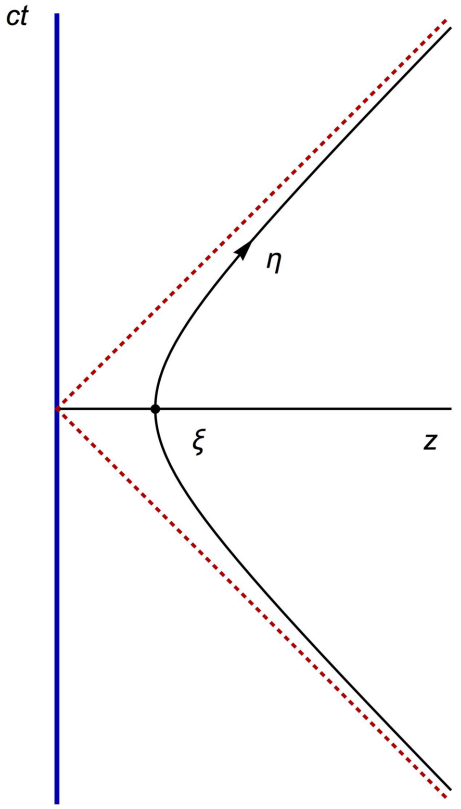

FIG. 2. Space-time diagram. The accelerated observer follows a hyperbola (curve) in space time. The observer comes in from ∞ with asymptotically $-c$, gets slower due to the acceleration in positive direction until coming to rest for a fleeting moment at $z = \xi$, and changing direction. Then the observer gains speed, asymptotically approaching $+c$ at ∞. The dotted lines indicate the causal cones straddled by the accelerated observer. The trajectory obeys Rindler's formula, Eq. (2), for constant ξ.

Note that the space-time trajectory (Fig. 2) must be processed with respect to the proper time [21] of the accelerated observer. Due to relativistic time dilatation [21] this time ticks exponentially slow when the observer moves with a speed close to c. In order to perform the spectral analysis for the Planck spectrum with Unruh temperature, sufficient proper time is required, during which the observer traverses exponentially large distances in an exponentially large laboratory time. These challenges are universal to all observations of the Unruh effect, but have not been met so far. We have confined the waves in a container and recorded the trajectory between two nodes of standing waves that acts as two mirrors. Taking mirror images of the space-time trajectory saves exponentially large laboratory space. For reducing the measurement time to the absolute minimum we have developed a form of Fourier analysis (Appendix B) where we directly read off the correlations in the Unruh effect that give the Planck spectrum.

These correlations are modified in an interesting way by the mirrors. In free space, an accelerated observer gets quantum-entangled with a partner if such a partner moves on the exact mirror image of the observer's trajectory [22,23]. Whenever the first observer records the click of a particle detector, so does the partner (assuming perfect detection efficiency). If the two paired observers use amplitude detectors, they record the two-mode squeezing [23] of Gaussian noise (Appendix A). In our case (Fig. 1) the boundary of the container acts like a mirror reflecting a hypothetical partner back onto the trajectory of the observer, which turns out to create single-mode squeezing of noise [23], an effect we have clearly observed experimentally.

Here, the noise for the real part of the Fourier components of the observed amplitudes is reduced, while the noise for the imaginary part is enhanced. The total excess noise follows a Planck spectrum with Unruh temperature [Eq. (1)]. It has been noticed before [24] that a mirror does not affect the thermal spectrum of the quantum Unruh effect, which was perceived as a paradox, because the mirror prevents the accelerated observer from getting entangled with unobserved parts of the quantum field. Where else would the excess entropy come from? In this paper we have found and demonstrated a mechanism for the accumulation of noise: single-mode squeezing.

Our findings suggest that at the heart of the Unruh effect lies the correlation of wave noise, regardless whether these waves are quantum or classical. Figure 1 (bottom) illustrates this idea. The figure shows the space-time diagram of water

waves subject to noise. Although the wave amplitudes are random in space, they are organized in space time: One clearly sees the causal cones of wave propagation, in addition to the reflections at the boundaries. This organization of wave noise in space and time generates the correlations in the Unruh effect that appear to a single observer as excess thermal energy with Unruh temperature [Eq. (1)].

II. THEORY

A. Uniform acceleration

Let us begin with a miniature review on accelerated observers for introducing the notation and for keeping the paper as self-contained as possible. Figure 2 shows the space-time diagram of the accelerated observer with position z at time t; the observer follows a hyperbola parametrized in terms of the Rindler coordinates [23,25] ξ and η as

$$z = \xi \cosh \eta, \quad ct = \xi \sinh \eta, \tag{2}$$

with constant ξ, and c being the speed of the waves. In the following we prove that the Rindler trajectory of Eq. (2) indeed describes constant acceleration [26]. Consider the effect of a Lorentz transformation to a frame moving with velocity u. Lorentz transformations are the hyperbolic rotations [21] $ct = ct' \cosh \chi + z' \sinh \chi$, $z = z' \cosh \chi + ct' \sinh \chi$ with

$$\tanh \chi = \frac{u}{c}. \tag{3}$$

Note that we replace c by the speed of the waves as before. We see from Eq. (2) that the Lorentz transformation leaves ξ invariant, but shifts the parameter η along the Rindler trajectory:

$$\eta = \eta' + \chi. \tag{4}$$

The entire Rindler trajectory can be drawn from some initial η' by a continuous succession of Lorentz boosts at uniform rate, i.e., by uniform acceleration. This proves with minimal technical effort that the Rindler trajectory is indeed the trajectory of constant acceleration.

It remains to find the physical meaning of the parameters ξ and η, and to calculate the value of the acceleration. We see from Eq. (2) and Fig. 2 that ξ describes the stopping distance of the trajectory—the point when the observer reaches a moment of rest. For finding the meaning of η, we express the Minkowski metric $ds^2 = c^2 dt^2 - dz^2$ in Rindler coordinates (2) and get $ds^2 = \xi^2 d\eta^2 - d\xi^2$. The metric s divided by c gives the proper time τ. Since on the Rindler trajectory ξ is constant, $d\xi = 0$, and so we obtain

$$\tau = \frac{\xi}{c}\,\eta. \tag{5}$$

The parameter η is thus proportional to the proper time τ as perceived by the accelerated observer. The acceleration is given by the derivative of the boost velocity from one frame to the next with respect to the time in the co–moving frame, i.e., with respect to proper time:

$$a = \left.\frac{du}{d\tau}\right|_{u=0} = c\,\frac{d\chi}{d\tau} = c\,\frac{d\eta}{d\tau} = \frac{c^2}{\xi}, \tag{6}$$

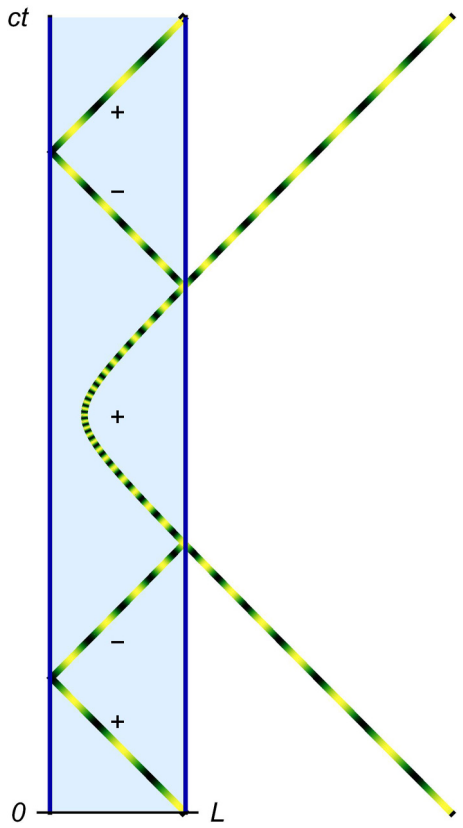

FIG. 3. Mirrors. Two reflecting boundaries or nodes, acting as mirrors, confine the waves between 0 and L. In this case, instead of tracing the full Rindler trajectory (Fig. 2) it is sufficient to scan its mirror images with the appropriate signs indicated. The pulsation along the space-time trajectory indicates the changing measure of time experienced by the accelerated observer. As time flows exponentially slowly for velocities approaching c, an exponentially large laboratory would be required to trace a sufficiently long trajectory, were it not for the mirrors.

using Eqs. (3)–(5). The acceleration is inversely proportional to the stopping distance ξ, as one might expect. We have thus proved that the Rindler trajectory describes uniform acceleration and derived the relationship of the Rindler parameters to the value of the acceleration.

B. Modes and noise

In our experiment, c is replaced by the speed of the water waves. We made another simplification that makes the experiment feasible (but is not essential to the classical analog of the Unruh effect—see Appendix A). The water channel cannot be infinitely extended, but shall have reflecting boundaries or nodes that act as mirrors for water waves (Fig. 3). The mirror on the left is placed at the origin ($z = 0$) of the Rindler frame—at the origin of the causal cone the accelerated observer straddles; the mirror at the right ($z = L$) is less important in principle, but very important in practice: As the two mirrors reflect the waves, one does not need to trace the entire Rindler trajectory, but only its reflections in the mirrors (Fig. 3). Since z grows exponentially with η, the pair of mirrors saves exponentially large laboratory space.

The amplitude A of the water surface can be understood as a superposition of modes A_k with coefficients α_k (assuming linear wave propagation):

$$A = \int_0^\infty (\alpha_k A_k + \alpha_k^* A_k^*)\, dk. \tag{7}$$

The mode coefficients α_k encode the physical state of the wave, including their noise. The coefficients are complex numbers written in terms of the quadratures q and p [23] as

$$\alpha = \frac{1}{\sqrt{2}}(q + ip). \tag{8}$$

We assume Gaussian noise of uniform strength I for the quadratures such that the averages $\langle q\rangle$, $\langle p\rangle$, and $\langle qp\rangle$ vanish, and

$$\langle q_1 q_2\rangle = \langle p_1 p_2\rangle = \frac{I}{2}\,\delta(k_1 - k_2). \tag{9}$$

For defining the strength of the noise we need to normalize the modes according to a certain time-invariant scale. For this we use the scalar product,

$$(A_1, A_2) = \frac{i}{c}\int \left(A_1^* \frac{\partial A_2}{\partial t} - A_2 \frac{\partial A_1^*}{\partial t}\right) dz, \tag{10}$$

that is invariant in time for modes satisfying the wave equation. The left mirror enforces the boundary condition $A_k = 0$ at $z = 0$ and thus selects from the plane waves with wave numbers k the superposition,

$$A_k = \mathcal{A}\sin(kz)\exp(-ikct). \tag{11}$$

These modes are normalized to $\delta(k_1 - k_2)$ according to the scalar product of Eq. (10) for

$$\mathcal{A} = \frac{1}{\sqrt{\pi k}}. \tag{12}$$

The right mirror at $z = L$ imposes

$$k = m\frac{\pi}{L}. \tag{13}$$

With this set of wave numbers the amplitude A would, mathematically, be a periodic function in space, $A(z + 2L) = A(z)$, and, as $A(-z) = -A(z)$, we have $A(z + L) = -A(L - z)$. This means that instead of scanning the entire trajectory of the accelerated observer, we only need to scan its reflections with the appropriate signs (Fig. 3).

C. Measured quantity

In the following we ignore the auxiliary right mirror (assuming a sufficiently dense set of modes). Suppose that a statistical ensemble of many videos of the waves are taken. In the original Unruh effect [1], a Planck spectrum with the temperature of Eq. (1) is predicted for the accelerated observer. In order to get information about the spectrum, we need to Fourier transform the recorded wave amplitudes along the Rindler trajectories of Eq. (2) and for the proper time as seen by the accelerated observer, Eq. (5), *i.e.* with respect to η:

$$\widetilde{A} = \int_{-\infty}^{+\infty} A\, \mathrm{e}^{\mathrm{i}\nu\eta}\, \mathrm{d}\eta\,. \tag{14}$$

This is the experimental quantity of interest we need to analyze and compare with the Unruh effect [1–3].

As the amplitude A is the superposition of modes A_k according to Eq. (7), we focus on one arbitrary mode, Eq. (11), and express it in the Rindler coordinates of Eq. (2):

$$A_k = \frac{\mathcal{A}}{2\mathrm{i}}[\exp(ik\xi e^{-\eta}) - \exp(-ik\xi e^{\eta})]. \tag{15}$$

Consider either of the two plane waves that constitute A_k [Fig. 4(a)] [26]. We obtain for the Fourier transform,

$$\widetilde{A_\pm} = \int_{-\infty}^{+\infty} \exp(\pm ik\xi e^{\mp\eta} + i\nu\eta)d\eta \tag{16}$$

$$= \mp(\mp ik\xi)^{\pm i\nu}\int_0^{\pm i\infty} e^{-x}x^{\mp i\nu - 1}dx$$

$$= -(k\xi)^{\pm i\nu}e^{\pi\nu/2}\,\Gamma(\mp i\nu), \tag{17}$$

where we substituted $x = \mp ik\xi\, e^{\mp\eta}$ in the first step and deformed the integration contour to the real axis in the second step, using there also the definition of the gamma function [27] and $(\mp i)^{\pm i\nu} = e^{\pi\nu/2}$. Now, turn to the Fourier integral of the complex conjugate plane wave:

$$\widetilde{A_\pm^*} = \int_{-\infty}^{+\infty} \exp(\mp ik\xi e^{\mp\eta} + i\nu\eta)d\eta. \tag{18}$$

Substituting $x = \pm ik\xi\, e^{\mp\eta}$ and using $(\pm i)^{\pm i\nu} = e^{-\pi\nu/2}$ in this case, one obtains the remarkable relation [28],

$$\widetilde{A_\pm^*} = e^{-\pi\nu}\widetilde{A_\pm}. \tag{19}$$

The factor $e^{-\pi\nu}$ is exponential in ν and independent of the mode index, which turns out to be the mathematical key to the thermality and universality of the Unruh effect.

Having obtained the results of Eqs. (17) and (19) for running plane waves [26], we turn to the standing waves of Eq. (15)—our modes [Fig. 4(b)]. We get for their Fourier transforms,

$$\widetilde{A_k} = -\mathcal{A}\,e^{\pi\nu/2}\mathrm{Im}[(k\xi)^{i\nu}\Gamma(-i\nu)]$$

$$= -e^{\pi\nu/2}\,\frac{\sin(\nu\ln k\xi - \phi)}{\sqrt{k\nu\sinh\nu\pi}}. \tag{20}$$

In the last step we have used Eq. (12) for $\mathcal{A}$ and the relationship $|\Gamma(i\nu)|^2 = \pi/(\nu\sinh\pi\nu)$ for the magnitude of the gamma function [27]; ϕ abbreviates the phase $\arg\Gamma(i\nu)$ [29]. For the Fourier transforms of the complex conjugate modes we have as before:

$$\widetilde{A_k^*} = e^{-\pi\nu}\widetilde{A_k}. \tag{21}$$

We substitute Eqs. (20) and (21) into the mode expansion, Eq. (7), of the Fourier integral, Eq. (14), and arrive at the expression,

$$\widetilde{A} = \int_0^\infty \frac{\sin(\phi - \nu\ln k\xi)}{\sqrt{k\nu\sinh\nu\pi}}\,(\alpha_k e^{\pi\nu/2} + \alpha_k^* e^{-\pi\nu/2})\,dk. \tag{22}$$

D. Squeezing and Planck spectrum

Let us analyze the quantity of interest $\widetilde{A}$. It is wise to combine the α_k in Eq. (22) in the total amplitude,

$$\alpha = \int_0^\infty \frac{\sin(\phi - \nu\ln k\xi)}{\sqrt{\pi k}}\,\alpha_k\,dk. \tag{23}$$

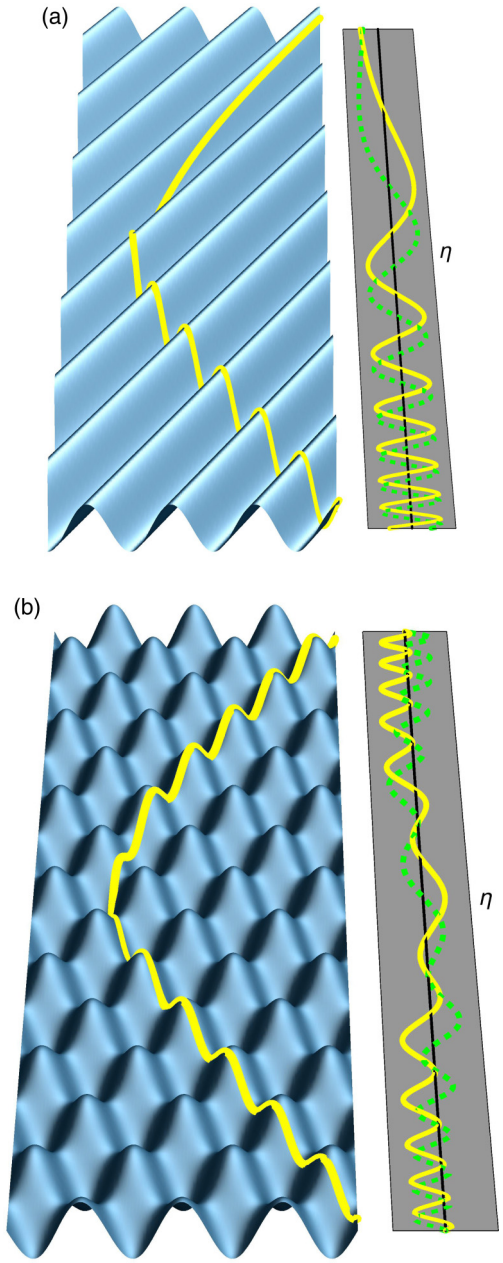

FIG. 4. Plane waves. (a) The accelerated observer (Fig. 2) traces a single running plane wave; on the side panel the real part (solid) and imaginary part (dotted) of the signal are plotted as functions of η. One sees exponentially rapid oscillations for $\eta \ll -1$ and an exponential freeze for $\eta \gg 1$. (b) The observer traces a standing wave. The real part (solid) is an even function in η, the imaginary part (dotted) is odd in η, both oscillate exponentially for $|\eta| \gg 1$.

Given that the individual mode amplitudes α_k represent Gaussian noise, the total amplitude α is Gaussian as well. Given the only nonvanishing second moments of Eq. (9) for the individual quadratures, the quadratures of the total amplitude must fluctuate with the same strength [30]:

$$\langle q(\nu_1)q(\nu_2)\rangle = \langle p(\nu_1)p(\nu_2)\rangle = \frac{I}{2}\,\delta(\nu_1-\nu_2). \tag{24}$$

Gaussian noise is completely characterized by the first and second moments, so the total mode amplitude α represents exactly the same noise as each of the individual mode amplitudes.

The amplitude α describes the total noise incident in one Fourier component of the detected signal, the total incident noise, but this is not the noise detected by the moving observer. To determine the detected noise we represent the exponential factor $e^{-\pi\nu}$ as

$$e^{-\pi\nu} = \tanh\zeta. \tag{25}$$

We express the Fourier transformed amplitude along the Rindler trajectory, Eq. (22), in terms of the total noise amplitude, Eq. (23), and its quadratures, Eq. (8), and arrive at the compact expressions,

$$\begin{aligned}\widetilde{A} &= \sqrt{\frac{2}{\nu}}\,(\alpha\cosh\zeta + \alpha^*\sinh\zeta)\\ &= \frac{1}{\sqrt{\nu}}(q\,e^{\zeta} + ip\,e^{-\zeta}).\end{aligned} \tag{26}$$

We see that the detected noise is squeezed—the noise in the p quadrature is reduced at the expense of the noise in the q quadrature [23]. The squeezing parameter $\Delta(\mathrm{Re}\widetilde{A})/\Delta(\mathrm{Im}\widetilde{A}) = e^{2\zeta}$ we easily obtain solving Eq. (25) for $e^{2\zeta}$:

$$\frac{\Delta(\mathrm{Re}\widetilde{A})}{\Delta(\mathrm{Im}\widetilde{A})} = \coth\frac{\pi\nu}{2}. \tag{27}$$

Note that although the detected noise is reduced in $\mathrm{Im}\widetilde{A}$, the total noise has grown:

$$\begin{aligned}\langle\widetilde{A}(\nu_1)\widetilde{A}^*(\nu_2)\rangle &= \frac{I}{2\nu}(e^{2\zeta} + e^{-2\zeta})\delta(\nu_1-\nu_2)\\ &= \frac{2}{\nu}\,I\left(\frac{1}{2} + \sinh^2\zeta\right)\delta(\nu_1-\nu_2).\end{aligned} \tag{28}$$

Here the $1/2$ represents the incident noise—the equivalent of the vacuum noise, while the $\sinh^2\zeta$ term accounts for the additional fluctuations perceived in total by the moving observer. We denote $\sinh^2\zeta$ by $\overline{n}$ and obtain from Eq. (25),

$$\overline{n} = \frac{1}{e^{2\pi\nu}-1}. \tag{29}$$

The Fourier component ν to the dimensionless Rindler parameter η is proportional to the frequency ω with respect to the proper time τ of the moving observer. We get from Eqs. (5) and (6),

$$\nu = \frac{\xi}{c}\,\omega = \frac{c}{a}\,\omega. \tag{30}$$

Reading $2\pi\nu$ in Eq. (29) as $\hbar\omega/k_{\mathrm{B}}T$ we see that the energy of the extra noise $\overline{n}$ follows a Planck distribution; using Eq. (30) we realize that its temperature T matches exactly the Unruh temperature of Eq. (1).

Our water-wave analog exactly reproduces the Unruh effect for the total fluctuations; the squeezing is due to the mirror. Without the mirror the signal along the Rindler trajectory would be correlated to the signal along the mirror image of the trajectory. The mirror projects these correlations into the Fourier quadratures of a single trajectory; two-mode squeezing [23] of noise turns into single-mode squeezing [23]. Our analog shows the essence of the correlations in the Unruh effect [22] with an interesting twist.

III. EXPERIMENT

A. Simplifications

We performed an experiment to test whether these ideas are robust under real laboratory conditions. For this, we simplified our scheme (Fig. 1) even further. Instead of taking the video of the height of the water surface at a moving spot representing the accelerated observer on a Rindler trajectory (Fig. 2), we took a video of the entire surface evolving in time. We then analyzed *a posteriori* the measured surface along Rindler trajectories, described by Eq. (2), varying ξ and hence, according to Eq. (6), the acceleration a.

We also did not apply white noise to the water, but rather created a standing wave through Faraday instability [31] by oscillating vertically the container. Such Faraday waves behave like laser light—they have stable average amplitudes due to the balance of gain and loss, but carry some amplitude noise. We randomized the phase by randomizing the initial time of the trajectories in the data analysis, for having a complete analog to laser light. With this, we studied the *stimulated* Unruh effect similar to the experiments [17] on the stimulated Hawking effect in water. The stimulated effect shares the characteristic features of the Unruh effect—the quadrature squeezing according to the Planck spectrum with the correct temperature [Eq. (1)]. This type of experiment has the advantage of avoiding dispersion—the wavelength dependance of c, because only one wavelength is used. Without dispersion, c is always well defined and can therefore be used without restriction as the basis for the Rindler trajectories of Eq. (2).

B. Experimental details

The details of the experiment are as follows. A standing wave field was created by exciting the Faraday instability [31] on the surface of a bath of plain tap water. The bath was vertically oscillated at a frequency of 19 Hz with an amplitude just above the instability threshold, giving rise to waves with a frequency of 9.5 Hz and a wavelength of 24 mm. The rectangular shape of the water cavity (250 mm $\times$ 55 mm) ensured that an approximately one-dimensional standing wave formed along the length of the container. The profile of the water surface was measured by tracking the optical distortions of a striped floor pattern (seen through the liquid) using a digital video camera (at 500 frames per second) and basic image processing. The resulting displacement field is proportional to the local slope of the water surface, which was numerically integrated to yield the height field [32]. The integration constant for each frame was determined from the conservation of mass. Data was taken for 1400 s. Figure 5 shows the standing-wave pattern for the first 100 cycles. The figure also shows the gradual decline of the average amplitude due to slow variations of the Faraday instability threshold; we corrected for this systematic decline in our data analysis.

C. Experimental results

Figure 6 shows the results of the data analysis obtained with the method described in Appendix B: half-odd Fourier transformation. We selected from the 1400 s of data 131 disjoined runs with 100 cycles each, choosing a random initial phase for each run, and correcting for the systematic decline in

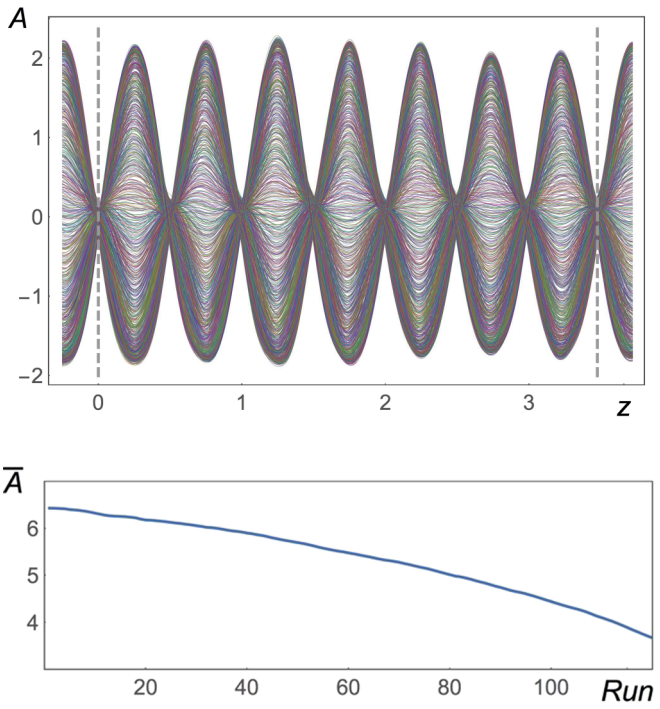

FIG. 5. Waves produced through Faraday instability. (Top) Measured wave amplitudes A in arbitrary units along z in units of wavelength for the first 100 cycles of wave propagation. The wave pattern continues to the left and right of the figure, but with decreasing amplitude. We selected two nodes of the standing waves as our mirrors (dashed lines). One sees that the waves are not perfectly harmonic—Fourier analysis (not shown here) reveals that anharmonicities contribute to about 10% of the amplitude. (Bottom) Decline of the average amplitude $\bar{A}$ over the runs of the experiment. Each run comprises 100 cycles with randomized initial phase in which the accelerated observer traverses a Rindler trajectory (Fig. 2). The quantity $\bar{A}$ we obtain for each run as the root-mean square of the entire wave amplitude between the mirrors with respect to space and time. We corrected for this decline in our data analysis.

average amplitude (bottom of Fig. 5). Each run represents an individual element of a statistical ensemble with random phase (and with some amplitude noise). We took a Rindler trajectory (Fig. 2) with fixed parameter ξ according to Eq. (2) and η running from -2π to $+2\pi$. When necessary, we mirrored the space-time trajectory (Fig. 3). Having chosen the trajectory, we calculated, for each run, the Fourier coefficients,

$$\widetilde{A} = \int_{-2\pi}^{+2\pi} A\, e^{i\nu\eta}\, d\eta, \tag{31}$$

for the first three half-odd Fourier numbers ν according to Eq. (B9): $\nu \in \{1/4, 3/4, 5/4\}$. Figure 6 displays the real and imaginary part of the half-odd Fourier coefficients and compares them with theory—the squeezed noise of a wave with fixed amplitude and random phase, with squeezing parameter given by Eq. (27). One sees that the experiment agrees reasonably well with theory for the first two Fourier coefficients, despite the imperfections of the experiment, in particular the anharmonic contributions to the waves (Fig. 5).

We quantified the squeezing energy and its spectrum as follows. We fitted centered ellipses to the data points of Fig. 6

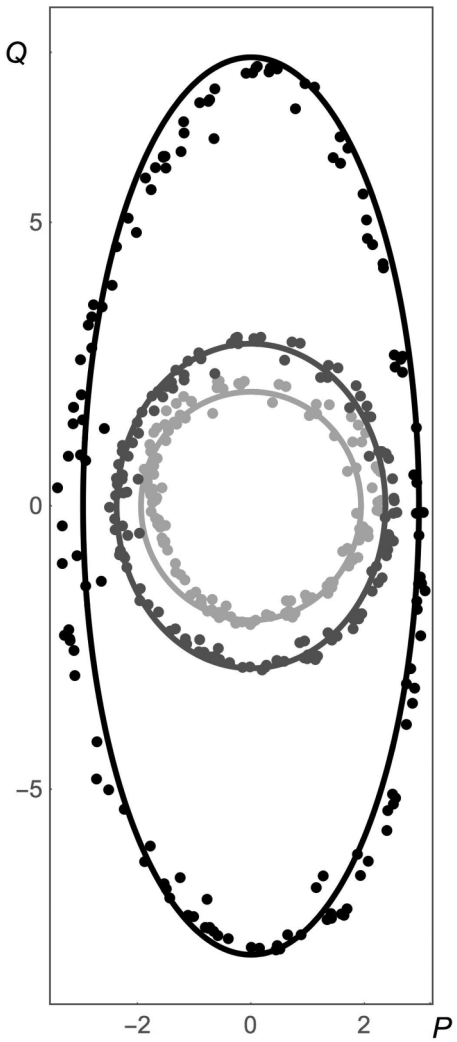

FIG. 6. Experimental results. The dots show the real and imaginary half-odd Fourier coefficients in the units of A (Fig. 5) for each run of the experimental data: black, $\nu = 1/4$; gray, $\nu = 3/4$; light gray, $\nu = 5/4$; $Q = \mathrm{Re}\widetilde{A}$, $P = \mathrm{Im}\widetilde{A}$. The Fourier coefficients are taken according to Eq. (31) along the space-time trajectory of an accelerated observer (Fig. 2). The ellipses represent the theory, assuming the squeezing of noise with fixed amplitude (matched with the data) and random phase; the squeezing parameter is given by Eq. (27).

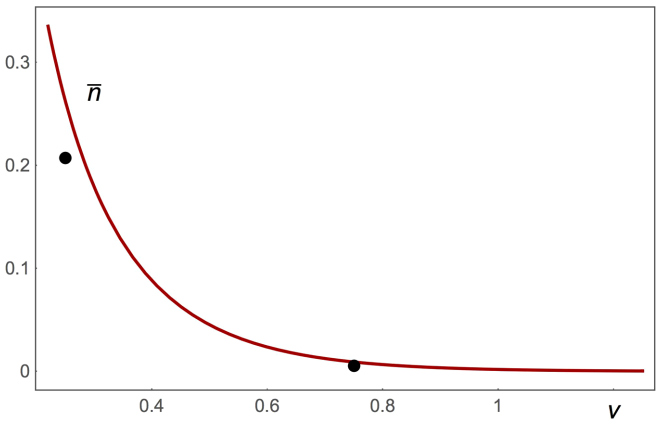

FIG. 7. Planck curve. (Dots) Squeezing energy and excess noise $\overline{n}$ calculated from the data (Fig. 6) for $\nu = 1/4$ and $\nu = 3/4$. To obtain the two dots shown here, centered ellipses are fitted to the two corresponding data sets of Fig. 6. From the ellipses the squeezing energy is calculated. (Curve) Theoretical prediction of a Planck curve according to Eq. (29). The experimental points lie remarkably close to the theoretical curve, despite clear deviations of the waves from harmonicity (Fig. 5), which illustrates the robustness of the Unruh effect against experimental imperfections.

by fitting a linear function $Q^2 = \Delta Q^2 - (\Delta Q/\Delta P)^2 P^2$ to the points, with $Q = \mathrm{Re}\widetilde{A}$ and $P = \mathrm{Im}\widetilde{A}$. The linear coefficient of the fit directly gives $\Delta Q/\Delta P = e^{\zeta}$, from which one obtains $\overline{n} = \sinh^2\zeta$. Note that in this way we extract the excess noise $\overline{n}$ from the squeezing and not directly from the amplitude fluctuations. We need to do this, because in our case—the case of the stimulated Unruh effect—the amplitude is dominated by the coherent amplitude of the waves we are probing. Our results are shown in Fig. 7 and compared with the Planck curve of Eq. (29).

From the statistical errors of the coefficients of the linear fit we determined the statistical errors of $(\Delta Q/\Delta P)^2$. We get 0.15 for $\nu = 1/4$ and 0.03 for $\nu = 3/4$. These errors are too small to explain the difference between the experimental values, 5.83 and 1.34, and the theoretical ones, 7.16 and 1.46, which shows that there are systematic errors in the data, most probably due to anharmonicities (Fig. 5). Nevertheless, the agreement with theory in the squeezing ellipses (Fig. 6) and in the Planck curve (Fig. 7) is still remarkable.

We varied ξ and did not see much principal variation in the results, except that the agreement with theory gets better the larger ξ is—the smaller the acceleration a is—according to Eq. (6). The reason is probably the following: For smaller a the space-time trajectory spends more proper time away from the node at $z = 0$ where contributions from anharmonicity and other noise matter most. Figure 6 shows our results for the maximal ξ we can accommodate for $-2\pi \leqslant \eta \leqslant +2\pi$ within 100 cycles of wave oscillations.

The third Fourier coefficient reveals the limits of the present experiment; there the subtle squeezing described by $\Delta(\mathrm{Re}\widetilde{A})/\Delta(\mathrm{Im}\widetilde{A}) = \coth(\pi\nu/2) \approx 1.04$ for $\nu = 5/4$ can no longer be resolved. Nevertheless, the squeezing energies for the first two coefficients establish the first two points anywhere near the Planck curve of the Unruh effect ever recorded (Fig. 7).

IV. COMMENTS

We have developed a theory that has revealed the classical root of the Unruh effect as the correlation of noise in space and time. We have demonstrated aspects of this theory in a simple laboratory experiment where we observed the squeezing of noise (Fig. 6). The excess noise of the squeezing lies near the ideal Planck curve of the Unruh effect for the first two measurable Fourier coefficients (Fig. 7). The experiment so far proves that the effect is robust, even in the presence of experimental imperfections (Fig. 5).

Improving the experiment significantly probably requires a different physical system that avoids anharmonicities and dispersion, such as waves on mechanical strings. With such a system one could probe the spontaneous Unruh effect as

described in our theory, and not only the stimulated effect. In such an experiment, one could see the Planck spectrum of the Unruh effect directly in the excess noise, and not infer it from the squeezing, as we have done in the present paper.

We note that the Unruh effect emerges in the correlations of wave noise; these correlations do exist regardless of the observer. The noise might be quantum or classical; it gets correlated due to wave propagation [Fig. 1(a)]. The observer is able to access those correlations on accelerated trajectories (Fig. 2) where different accelerations correspond to different effective temperatures according to Unruh's formula [Eq. (1)]. It is therefore sufficient to record the entire noise field and then to analyze the data, following the space-time trajectories of accelerated observers, as we did in our experiment.

Apart from the first experimental demonstration of a stimulated Unruh effect, our classical analog may also stimulate further discussions on some of the more speculative facets of the effect. One may view the Unruh effect as a manifestation of the quantum vacuum as a physical substance: The quantum vacuum appears as the modern ether. It is Lorentz invariant—in agreement with relativity—but not invariant under accelerations. One may view this as a manifestation of inertia, distinguishing between uniform, inertial motion, and accelerated, noninertial motion. In resisting acceleration, the Unruh effect may explain deviations from acceleration that mimic the behavior of hypothetical dark matter [33]. Our classical analog may show how to generalize this idea to trajectories of nonuniform accelerations. Here a straightforward extension of the quantum result is difficult, but our classical concepts still hold.

The classical analog of the Unruh effect may also serve in Jacobson's thermodynamic derivation [34] of Einstein's equations of gravity [21]. Like Bekenstein's black-hole thermodynamics [4] that assigns an entropy to the area of the event horizon of the black hole with the Hawking temperature [5] as thermodynamic temperature, Jacobson assigned an entropy to any causal horizon with the Unruh temperature as thermodynamic temperature, and derived [34] from these assumptions Einstein's field equations [21]. There both the entropy and the temperature carry $\hbar$'s that cancel each other. Our findings imply that the entire argument can be made classical.

Note that Jacobson's thermodynamic derivation [34] establishes an alternative to the usual derivation of Einstein's equations from the principle of least action [21]. In our opinion [35] the action principle gives the strongest argument in favor of the existence of a quantum theory of gravity, because action principles normally arise due to the quantum interference of paths or field configurations. Jacobson's derivation, combined with the classical Unruh effect, opens another, equally credible route to Einstein's classical theory of gravity [21] avoiding the action principle altogether. On quantum gravity, it thus puts a question mark.

ACKNOWLEDGMENTS

We thank Rachel Bruch and Mordehai Milgrom for stimulating discussions. Our work was supported by the AXA research fund and LABEX WIFI (Grant No. ANR-10-LABX-24) within the French Program Investments for the Future (Grant No. ANR-10- IDEX-0001-02 PSL), the European Research Council and the Israel Science Foundation, a research grant from Louis Rosenmayer and from James Nathan, and the Murray B. Koffler Professorial Chair. I.G. is grateful to the Azrieli Foundation for support through an Azrieli Fellowship.

U.L. and I.G. contributed equally to this work, U.L. to the theory and I.G. to the data analysis of the experiment.

APPENDIX A: FREE WAVES

In this Appendix we consider the ideal case of free waves of Gaussian noise not constrained by boundaries (mirrors). We will establish the complete analogy to the Unruh effect and shall see the similarities and differences between the ideal case and the realistic case discussed in the main body of this paper.

We assume, as usual, that the wave field A is given by a superposition of modes,

$$A = \int_0^\infty \sum_{s=\pm} (\alpha_{sk} A_{sk} + \alpha_{sk}^* A_{sk}^*)\, dk, \tag{A1}$$

but now these modes are free plane waves where "+" refers to right-moving and "−" to left-moving waves:

$$A_{\pm k} = \mathcal{A} \exp(\pm ikz - kct) \tag{A2}$$

$$= \mathcal{A} \exp(\pm ik\xi\, e^{\mp\eta}), \tag{A3}$$

in Rindler coordinates, Eq. (2). Requiring the modes to be normalized to $\delta(k_1 - k_2)$ with respect to the scalar product of Eq. (10) we obtain from Eq. (A2),

$$\mathcal{A} = \frac{1}{\sqrt{4\pi k}}. \tag{A4}$$

For the mode coefficients α_{sk} we assume Gaussian noise of strength I such that

$$\langle \alpha_{s_1 k_1} \alpha_{s_2 k_2}^* \rangle = \frac{I}{2}\, \delta_{s_1 s_2}\, \delta(k_1 - k_2). \tag{A5}$$

It is easy to see that this Gaussian wave noise is Lorentz invariant (with the speed of the waves c playing the role of the speed of light). From the Lorentz transformation Eq. (4) and Eqs. (A3) and (A4) it follows that if we put

$$k' = k\, e^{\mp\chi}, \quad \alpha'_{\pm k} = e^{\mp\chi/2} \alpha_{\pm k}, \tag{A6}$$

we get exactly the same expressions for the modes and mode coefficients in terms of the k' as before for the k, including

$$\langle \alpha'_{s_1 k_1'} \alpha'^*_{s_2 k_2'} \rangle = \frac{I}{2}\, e^{-s\chi}\, \delta_{s_1 s_2}\, \delta(e^{-s\chi}(k_1' - k_2'))$$

$$= \frac{I}{2}\, \delta_{s_1 s_2}\, \delta(k_1' - k_2'). \tag{A7}$$

This proves the Lorentz invariance of the Gaussian wave noise. Note that Eq. (A6) describes the Doppler effect for the frequency ck, and the corresponding change in the noise amplitudes such that the total noise is invariant. Note also that the mirror used in the main body of the paper breaks the Lorentz invariance, because in a moving frame the mirror moves, which causes differences for both quantum and classical noise.

Consider now the noise as seen by accelerated observers. Imagine two observers on conjugate Rindler trajectories

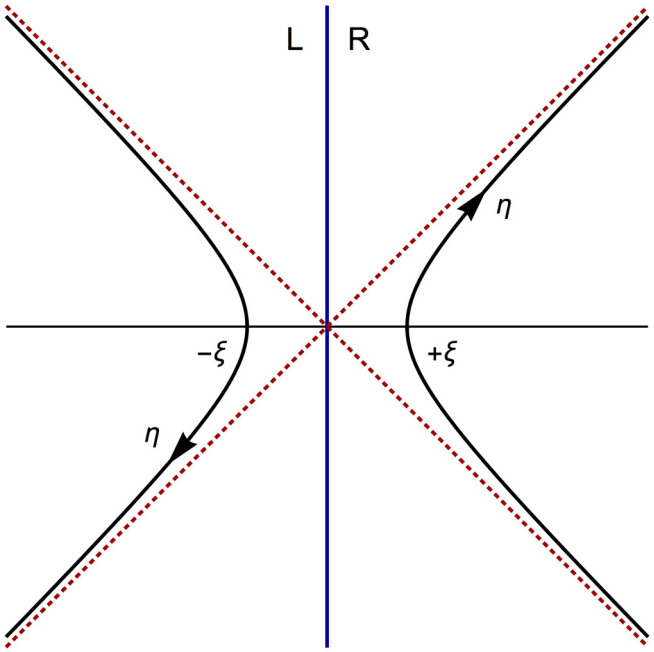

FIG. 8. Space-time diagram of conjugate accelerated observers. The observer on the right (R) is on a Rindler trajectory with constant positive ξ as in Fig. 2 and described by Eq. (2). The observer on the left (L) moves on the conjugate trajectory with $-\xi$ instead of ξ. In this case the η parameter must run backward for the proper time to be running forward; see Eq. (5). The two conjugate observers turn out to be correlated by the wave noise; see Eq. (A9).

(Fig. 8)—on the right side (R) one on the same trajectory as in Fig. 2 and on the left side (L) another one on the exact mirror image of the right observer's trajectory, $\xi \to -\xi$. Note that for the left observer proper time runs forward when η runs backward, as we see from Eq. (5) for negative ξ. The quantities of interest are

$$\widetilde{A}_{\rm R} = \int_{-\infty}^{+\infty} A({\rm R})\, e^{+i\nu\eta}\, {\rm d}\eta = \frac{\alpha_{\rm R}}{\sqrt{\nu}},$$
$$\widetilde{A}_{\rm L} = \int_{-\infty}^{+\infty} A({\rm L})\, e^{-i\nu\eta}\, d\eta = \frac{\alpha_{\rm L}}{\sqrt{\nu}}, \qquad \text{(A8)}$$

where R and L indicate the two trajectories taken. Along the same lines as in Sec. II C we obtain

$$\alpha_{\rm R} = \alpha_r \cosh\zeta + \alpha_l^* \sinh\zeta,$$
$$\alpha_{\rm L} = \alpha_l \cosh\zeta + \alpha_r^* \sinh\zeta, \qquad \text{(A9)}$$

where ζ is defined by Eq. (25) and

$$\alpha_r = \frac{\alpha_{+r} + \alpha_{-r}}{\sqrt{2}}, \quad \alpha_l = \frac{\alpha_{+l} + \alpha_{-l}}{\sqrt{2}}, \qquad \text{(A10)}$$

with the noise coefficients,

$$\alpha_{\pm r} = -e^{\mp i\phi} \int_0^\infty \frac{(k\xi)^{\pm i\nu}}{\sqrt{2\pi k}}\, \alpha_{\pm k}\, dk\,,$$
$$\alpha_{\pm l} = -e^{\pm i\phi} \int_0^\infty \frac{(k\xi)^{\mp i\nu}}{\sqrt{2\pi k}}\, \alpha_{\pm k}\, dk. \qquad \text{(A11)}$$

We get for Gaussian noise in the amplitudes $\alpha_{\pm k}$ with correlators given by Eq. (A5):

$$\langle \alpha_{\pm r}(\nu_1)\, \alpha_{\pm r}^*(\nu_2)\rangle = \frac{I}{4\pi} \int_0^\infty (k\xi)^{\pm i(\nu_1-\nu_2)}\, \frac{dk}{k}$$
$$= \frac{I}{2}\, \delta(\nu_1 - \nu_2), \qquad \text{(A12)}$$

and the same for $\langle \alpha_{\pm l}(\nu_1)\, \alpha_{\pm l}^*(\nu_2)\rangle$, while the correlators with different s or with mixed r and l vanish. This shows that the $\alpha_{\pm r}$ and $\alpha_{\pm l}$ are subject to the same Gaussian noise as the original mode coefficients $\alpha_{\pm k}$ with ν playing the role of k. The Hadamard transform of Eq. (A10) does not change this either. Hence the heart of the Unruh effect in the Gaussian wave noise is the two-mode squeezing transformation [23] described by Eq. (A9).

This is exactly the same transformation as in the quantum Unruh effect [1,23] and hence it has the same consequences. The two modes measured by the two accelerated observers are correlated as in the Einstein-Podolsky-Rosen paradox [23,36]—the q quadratures are directly correlated while the p quadratures are anticorrelated. When projected onto one of the two observer modes the wave noise appears in a thermal state [23] with Planck spectrum and Unruh temperature [Eq. (1)]. The classical Unruh effect for free waves and the quantum Unruh effect are in perfect analogy.

APPENDIX B: HALF-ODD FOURIER TRANSFORMATION

The main difficulty of the data analysis for our—and probably all other experimental attempts to measure the Unruh effect—comes from the extreme time dilatation experienced by the accelerated observer. The laboratory time t along the Rindler trajectory (2) depends exponentially on the proper time (5) for large η, as $\sinh\eta \sim e^\eta/2$. So in order to resolve the Planck spectrum, an exponentially large time is required (but thanks to the mirrors not an exponentially large laboratory space—Fig. 3). One resolves the Planck spectrum if the characteristic factor $e^{-\pi\nu}$ is resolved between the Fourier-transformed modes and the Fourier transforms of their complex conjugates. For achieving this, the resolution $\Delta\nu$ must be in the order of

$$\Delta\nu = \frac{1}{2\pi}. \qquad \text{(B1)}$$

We obtain from the time-frequency uncertainty relation, $\Delta\nu\,\Delta\eta \sim 1$, that $\Delta\eta \sim 2\pi$, which sets the minimal time window required for measuring the Planck spectrum.

Suppose a signal along the trajectory of the accelerated observer is detected. One needs to Fourier transform and possibly filter this signal. We assume that the signal is multiplied with a filter function F that describes both the finite observation time and the filtering:

$$A_{\rm F} = F(\eta)\, A(\eta). \qquad \text{(B2)}$$

In the Fourier transform, F appears as the convolution,

$$\widetilde{A}_{\rm F} = \frac{1}{2\pi} \int_{-\infty}^{+\infty} \widetilde{F}(\mu)\, \widetilde{A}(\nu-\mu)\, d\mu. \qquad \text{(B3)}$$

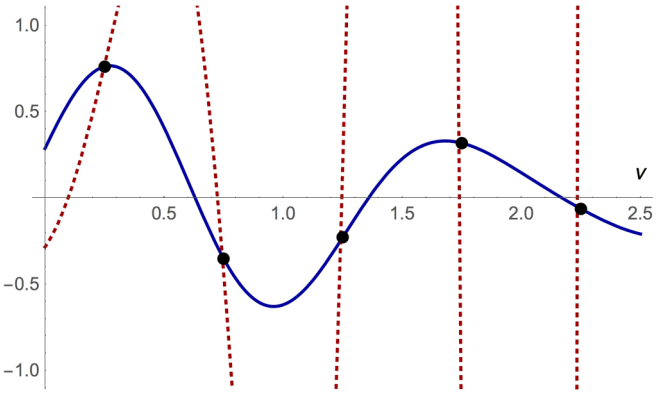

FIG. 9. Half-odd Fourier analysis. The signal [Fig. 4(b), $m = 10$, $\xi = 0.001L$] was Fourier–transformed in the minimal observation window $\eta \in \{-2\pi, +2\pi\}$. The Fourier-transformed signals were compared for the mode (solid curve) and its complex conjugate divided by the characteristic exponential $e^{-\pi\nu}$ (dotted). One sees that the two curves only agree, to a very good approximation, at the half-odd Fourier components (points) of Eq. (B9). For these Fourier components one can measure with minimal observation time a nearly perfect Planck spectrum with Unruh temperature [Eq. (1)].

The most efficient way of taking data is without filtering at all:

$$F(\eta) = \Theta(\eta + \Delta\eta)\,\Theta(\Delta\eta - \eta), \tag{B4}$$

where F only reflects the finite observation time we put to the minimal,

$$\Delta\eta = \frac{1}{\Delta\nu} = 2\pi. \tag{B5}$$

However, avoiding filtering completely produces a problem: The Fourier transform of the finite observation window contains long, oscillatory wings:

$$\widetilde{F} = \frac{2\sin(\nu/\Delta\nu)}{\nu}. \tag{B6}$$

Furthermore, according to Eq. (20), each Fourier-transformed mode has a pole at $\nu = 0$. The convolution of the wings of the Fourier-transformed filter function with the pole completely obscures the Planckian relationship of Eq. (21), unless the pole contribution vanishes (Fig. 9).

Consider a single pole at $\nu = 0$; imagine that $\widetilde{A}$ in the convolution (B3) is replaced by the pole. In this case the convolution integral takes the shape of the Hilbert transform [37] (Kramers-Kronig relation),

$$\mathrm{Re}\, f = \frac{1}{\pi}\int_{-\infty}^{+\infty} \frac{\mathrm{Im}\, f(\mu)}{\nu - \mu}\, d\mu, \tag{B7}$$

for complex functions f analytic on the upper half plane. Such a function is $(2/\nu)\exp(i\nu/\Delta\nu)$ with the desired imaginary part (B6) and the real part,

$$\mathrm{Re}\, f = \frac{2\cos(\nu/\Delta\nu)}{\nu}. \tag{B8}$$

The real part, and hence the convolution of the pole, vanishes for

$$\nu = \frac{2n+1}{2}\,\pi\Delta\nu = \frac{2n+1}{4} \quad \text{with} \quad n \in \mathbb{N}. \tag{B9}$$

For filtering out the pole one should thus use finite Fourier analysis at *half odd integers*—just between the usual Fourier components of periodic functions.

[1] W. G. Unruh, Notes on black-hole evaporation, Phys. Rev. D **14**, 870 (1976).

[2] S. A. Fulling, Nonuniqueness of canonical field quantization in riemannian space time, Phys. Rev. D **7**, 2850 (1973).

[3] P. C. W. Davies, Scalar production in Schwarzschild and Rindler metrics, J. Phys. A **8**, 609 (1975).

[4] J. D. Bekenstein, Black Holes and Entropy, Phys. Rev. D **7**, 2333 (1973).

[5] S. W. Hawking, Black hole explosions? Nature (London) **248**, 30 (1974).

[6] See e.g. L. C. B. Crispino, A. Higuchi, and G. E. A. Matsas, The Unruh effect and its applications, Rev. Mod. Phys. **80**, 787 (2008).

[7] W. G. Unruh, Experimental Black-Hole Evaporation? Phys. Rev. Lett. **46**, 1351 (1981); G. Volovik, *The Universe in a Helium Droplet* (Oxford University Press, Oxford, 2003); C. Barcelo, S. Liberati, and M. Visser, Analogue gravity, Living Rev. Relativity **8**, 12 (2005); W. G. Unruh and R. Schützhold (eds.) *Quantum Analogues: From Phase Transitions to Black Holes and Cosmology* (Springer, Berlin, 2007); D. Faccio, F. Belgiorno, S. Cacciatori, V. Gorini, S. Liberati, and U. Moschella (eds.) *Analogue Gravity Phenomenology: Analogue Spacetimes and Horizons, from Theory to Experiment*, Lecture Notes in Physics 870 (Springer, Cham, 2013).

[8] A. Retzker, J. I. Cirac, M. B. Plenio, and B. Reznik, Methods for Detecting Acceleration Radiation in a Bose-Einstein Condensate, Phys. Rev. Lett. **101**, 110402 (2008).

[9] A. Iorio and G. Lambiase, The Hawking–Unruh phenomenon on graphene, Phys. Lett. B **716**, 334 (2012); Quantum field theory in curved graphene spacetimes, Lobachevsky geometry, Weyl symmetry, Hawking effect, and all that, Phys. Rev. D **90**, 025006 (2014); M. Cvetič and G. W. Gibbons, Graphene and the Zermelo optical metric of the BTZ black hole, Ann. Phys. (NY) **327**, 2617 (2012); P. Chen and H. Rosu, Note on Hawking-Unruh effects in graphene, Mod. Phys. Lett. A **27**, 1250218 (2012).

[10] T. Needham, *Visual Complex Analysis* (Clarendon Press, Oxford, 2002).

[11] J. Rodríguez-Laguna, L. Tarruell, M. Lewenstein, and A. Celi, Synthetic Unruh effect in cold atoms, Phys. Rev. A **95**, 013627 (2017).

[12] In the Unruh effect in odd space-time dimensions (even spatial dimensions), bosons appear as fermions and vice versa, see S. Takagi, Vacuum noise and stress induced by uniform acceleration: Hawking-unruh effect in rindler manifold of arbitrary dimension, Prog. Theor. Phys. Suppl. **88**, 1 (1986); this is also true for Dirac electrons in the Beltrami trumpet [10] made of graphene as proposed in Ref. [9].

[13] T. H. Boyer, Thermal effects of acceleration for a classical dipole oscillator in classical electromagnetic zero-point radiation, Phys. Rev. D **29**, 1089 (1984).

[14] A. Higuchi and G. E. A. Matsas, Fulling-Davies-Unruh effect in classical field theory, Phys. Rev. D **48**, 689 (1993).

[15] M. Pauri and M. Vallisneri, Classical roots of the Unruh and Hawking effects, Found. Phys. **29**, 1499 (1999).

[16] G. Cozzella, A. G. S. Landulfo, G. E. A. Matsas, and D. A. T. Vanzella, Proposal for Observing the Unruh Effect using Classical Electrodynamics, Phys. Rev. Lett. **118**, 161102 (2017).

[17] This is inspired by experiments for measuring the classical analog of Hawking radiation with water waves: S. Weinfurtner, E. W. Tedford, M. C. J. Penrice, W. G. Unruh, and G. A. Lawrence, Measurement of Stimulated Hawking Emission in an Analogue System, Phys. Rev. Lett. **106**, 021302 (2011); L-P. Euvé, F. Michel, R. Parentani, and G. Rousseaux, Wave blocking and partial transmission in subcritical flows over an obstacle, Phys. Rev. D **91**, 024020 (2015).

[18] L.-P. Euvé, F. Michel, R. Parentani, T. G. Philbin, and G. Rousseaux, Observation of Noise Correlated by the Hawking Effect in a Water Tank, Phys. Rev. Lett. **117**, 121301 (2016).

[19] U. Leonhardt, *Measuring the Quantum State of Light* (Cambridge University Press, Cambridge, 1997).

[20] D. T. Smithey, M. Beck, M. G. Raymer, and A. Faridani, Measurement of the Wigner Distribution and the Density Matrix of a Light Mode Using Optical Homodyne Tomography: Application to Squeezed States and the Vacuum, Phys. Rev. Lett. **70**, 1244 (1993).

[21] L. D. Landau and E. M. Lifshitz, *The Classical Theory of Fields* (Butterworth-Heinemann, Amsterdam, 2003); P. A. M. Dirac, *General Theory of Relativity* (Princeton University Press, Princeton, 1996).

[22] S. Massar and P. Spindel, Einstein-Podolsky-Rosen correlations between two uniformly accelerated oscillators, Phys. Rev. D **74**, 085031 (2006); see also B. Reznik, Entanglement from the vacuum, Found. Phys. **33**, 167 (2003); B. Reznik, A. Retzker, and J. Silman, Violating Bell's inequalities in vacuum, Phys. Rev. A **71**, 042104 (2005).

[23] U. Leonhardt, *Essential Quantum Optics: From Quantum Measurements to Black Holes* (Cambridge University Press, Cambridge, 2010).

[24] C. Rovelli and M. Smerlak, Unruh effect without trans-horizon entanglement, Phys. Rev. D **85**, 124055 (2012).

[25] W. Rindler, Kruskal Space and the Uniformly Accelerated Frame, Am. J. Phys. **34**, 1174 (1966).

[26] See also P. M. Alsing and P. W. Milonni, Simplified derivation of the Hawking-Unruh temperature for an accelerated observer in vacuum, Am. J. Phys. **72**, 1524 (2004).

[27] A. Erdélyi, W. Magnus, F. Oberhettinger, and F. G. Tricomi, *Higher Transcendental Functions* (McGraw-Hill, New York, 1981).

[28] One also sees this from the stationary phases in the Fourier integrals (16) and (18). The phase $\varphi = \pm k\xi e^{\mp\eta} + \nu\eta$ of integral (16) becomes stationary ($d\varphi/d\eta = 0$) for one point η at the real axis, but not the phase $\varphi_* = \mp k\xi e^{\mp\eta} + \nu\eta$ of integral (18). However, by going to $\eta + i\pi$ the phase φ_* becomes the same as φ, apart from $i\pi\nu$ that results in the exponential factor (19).

[29] One obtains from the method of stationary phase [28] $\phi \sim \nu \ln \nu - \nu - \pi/4$ for large ν.

[30] Expanding the sine in Eq. (23) into exponentials one gets for $\langle q(\nu_1)q(\nu_2)\rangle$ and also for $\langle p(\nu_1)p(\nu_2)\rangle$ the expression

$$\frac{I}{8\pi}\int_0^\infty (e^{i(\nu_1-\nu_2)\ln k\xi} + e^{i(\nu_2-\nu_1)\ln k\xi})\frac{dk}{k} = \frac{I}{2}\delta(\nu_1 - \nu_2)$$

that gives Eq. (24).

[31] M. Faraday, On a peculiar class of acoustical figures; and on certain forms assumed by groups of particles upon vibrating elastic surfaces, Philos. Trans. R. Soc. London **121**, 299 (1831); S. Douady, Experimental study of the Faraday instability, J. Fluid Mech. **221**, 383 (1990).

[32] H. Murase, Surface shape reconstruction of an undulating transparent object, in *Proceedings of the 3rd International Conference Computer Vision* (IEEE, Piscataway, 1990), pp. 313–317; F. Moisy, M. Rabaud, and K. Salsac, A synthetic Schlieren method for the measurement of the topography of a liquid interface, Exp. Fluids **46**, 1021 (2009).

[33] M. Milgrom, The modified dynamics as a vacuum effect, Phys. Lett. A **253**, 273 (1999).

[34] T. Jacobson, Thermodynamics of Spacetime: The Einstein Equation of State, Phys. Rev. Lett. **75**, 1260 (1995).

[35] U. Leonhardt, Cosmology in the laboratory: Challenges at the horizon in M. McCall *et al.*, Roadmap on Transformation Optics, J. Opt. **20**, 063001 (2018).

[36] A. Einstein, N. Rosen, and B. Podolsky, Can Quantum-Mechanical Description of Physical Reality Be Considered Complete? Phys. Rev. **47**, 777 (1935).

[37] M. J. Ablowitz and A. S. Fokas, *Complex Variables: Introduction and Applications* (Cambridge University Press, Cambridge, 2003).